Batteries & Supercaps

Research Article
doi.org/10.1002/batt.202300404

Chemistry Europe
European Chemical Societies Publishing

www.batteries-supercaps.org

Impact of Nano-sized Inorganic Fillers on PEO-based Electrolytes for Potassium Batteries

Anna D. Khudyshkina,[a] Ulf-Christian Rauska,[a] Andreas J. Butzelaar,[b] Maxi Hoffmann,[b] Manfred Wilhelm,[b] Patrick Theato,[b, c] and Fabian Jeschull*[a]

The low melting points of solid polymer electrolytes (SPEs) based on the KTFSI electrolyte salt allow comparatively low operation temperatures (below 50 °C) for K-ion batteries, unlike their Li or Na counterparts. Unfortunately, for this reason the electrolyte is also rendered mechanically unsuitable in its function to act as a cell separator. Therefore, in this work the use of inorganic nanofillers (Al_2O_3 and SiO_2) is explored with the aim to improve rheological, thermal and cation transport properties of the resulting polymer composite electrolytes. Their electrochemical properties were further examined in K-metal symmetrical cells and K-metal/SPE/$K_2Fe[Fe(CN)_6]$ cells and compared to corresponding liquid electrolyte systems. As a result of particle-polymer interactions, filler-containing SPEs showed higher degrees of crystallinity combined with filler polymer interaction and thus improved mechanical integrity in the relevant temperature range of 25–55 °C, while maintaining similar ionic conductivities than a filler-free sample above the melting temperature. Although plating-stripping experiments in symmetrical cell setups suggested high cell resistances for various compositions and in some cases even rapid cell failure, Al_2O_3-based SPEs generally displayed high capacity retention when cycled against a positive electrode (here Prussian blue analogue $K_2Fe[Fe(CN)_6]$) over 100–160 cycles and possibly beyond.

Introduction

In recent years, potassium-ion batteries (KIBs) have drawn great attention as a complementary post-Li technology.[1–3] Despite higher atomic mass of potassium, KIBs could be attractive energy storage systems especially if high average cell voltages above 4.0 V and a high stoichiometric content can be achieved.[2,4,5] Major bottlenecks to reliable KIBs are stable interface chemistries, the high reactivity of potassium towards electrolyte components.[6–9] The combination of the two leads to significantly more electrolyte degradation and thus rapid increase of the surface layer thickness and cell resistance, as well as fast capacity fade.[7,10] In addition, the availability of well-performing negative and positive electrode materials is limited. Graphite[4,10–12] and Prussian white-based compounds[13–16] are currently the most commonly used electrode materials due to their availability and comparatively high reversibility.

Several recent studies demonstrate that solid polymer electrolytes (SPEs) improved the capacity retention of half cell configurations notably compared to conventional carbonate-based liquid electrolytes (LEs).[17–21] Poly(ethylene oxide), PEO as a semi crystalline host material is the most prominent example for SPE applications owing to its ability to dissolve high amounts of electrolyte salt, leading to the formation of semi-crystalline polymer-salt complexes with high ion mobility at elevated temperatures.[22] Please note that even in the crystalline state of pure PEO there is a high molecular mobility within the crystallite due to fast jump motions along the helical screw.[23] Dissolution of salt in PEO is facilitated if the dissociation energy of the salt is low. Therefore, salts with bulky anions, such as bis(trifluoromethanesulfonyl)imide (TFSI), are commonly used. As ion transport mainly takes place in the amorphous phase[24] it is beneficial that bulky anions also have plasticising effects (lowering the glass transition temperature, T_g) and supress crystallisation. PEO exhibits high cathodic stability,[25,26] which is an important parameter when using reactive metallic negative electrode. However, in contact with high-voltage cathodes degradation processes commence in the voltage range around 4.3–4.6 V vs. Li^+/Li.[26,27] In our previous work,[17] comparatively high room temperature ionic conductivities of up to 3.0×10^{-5} S cm^{-1} were found for PEO-KTFSI compositions with ethylene oxide (EO)-to-potassium molar ratios (EO:K) of 16:1 and 12:1. The 12:1 composition showed an exceptionally low melting point, T_m, of 40 °C, but liquid like behaviour rendering the formulation unsuitable for SPE applications, as the SPE also has to fulfil the important role of a separator and thus requires certain mechanical strength to prevent short-circuits.

[a] A. D. Khudyshkina, U.-C. Rauska, Dr. F. Jeschull
Karlsruhe Institute of Technology (KIT), Institute for Applied Materials – Energy Storage Systems (IAM-ESS), Hermann-von-Helmholtz-Platz 1, 76344 Eggenstein-Leopoldshafen, Germany
E-mail: fabian.jeschull@kit.edu

[b] Dr. A. J. Butzelaar, Dr. M. Hoffmann, Prof. Dr. M. Wilhelm, Prof. Dr. P. Theato
Karlsruhe Institute of Technology (KIT), Institute for Chemical Technology and Polymer Chemistry (ITCP), Engesserstraße 18, 76131 Karlsruhe, Germany

[c] Prof. Dr. P. Theato
Karlsruhe Institute of Technology (KIT), Soft Matter Synthesis Laboratory – Institute for Biological Interfaces III (IBG-3), Hermann-von-Helmholtz-Platz 1, 76344 Eggenstein-Leopoldshafen, Germany

Supporting information for this article is available on the WWW under https://doi.org/10.1002/batt.202300404

The strategies to improve mechanical integrity of PEO-based electrolytes include for example chemical cross-linking,[28,29] or the use of multiphase structures as in graft or physical cross linking via block copolymeric materials,[30–34] additionally comprising a polymer possessing high T_g. We have followed the latter approach recently, using a PEO-based block copolymer[18] we were able to greatly improve the mechanical properties of the SPE, despite using an EO:K molar ratio of 15:1 in the liquid-like compositional regime. The addition of an inactive phase, however, came at the expense of lower ionic conductivities. Therefore, in this work, the addition of ceramic nanofillers to the PEO-KTFSI matrix was examined as an alternative approach to improve the mechanical properties.

Nano-sized inorganic fillers, such as Al_2O_3, SiO_2, TiO_2, ZrO_2, CeO_2, etc.[35–37] have been used in Li- and Na-SPEs with the aim to lower the crystallinity[38] and to enhance ion mobility through particle-polymer and particle-ion Lewis-acid-base interactions.[37,39–41] In case of attractive filler-polymer interactions confinement effect along the particle interface would be expected that restrict polymer chain mobility,[42,43] which is reflected in elevated T_g. According to literature, ion mobility can increase in such particle-polymer interface regions through formation of conducting pathways and restricted chain movement, but strongly depends on the dominating interactions between the individual components, as well as factors such as fillers size, its distribution and concentration.[36,39,41,44]

To study the impact of nanofillers on a PEO-KTFSI SPE with EO:K = 12:1 (as a promising ion-conducting formulation from our previous study[17]), we herein investigated thermal, rheological and ion transport properties of PEO-KTFSI composites comprising either nano-sized Al_2O_3 or SiO_2 fillers, respectively. Furthermore, electrochemical properties were studied in K/K symmetrical cells and K/K_{2-x}Fe[Fe(CN)$_6$] (denoted as KFF) half cells to determine the cathodic stability of the electrolytes and their capacity retention and Coulombic efficiencies over up to 160 cycles. In an optimized configuration, the K/KFF cell with filler-containing PEO-KTFSI electrolyte delivered an outstanding capacity retention of 99% even after 100 cycles.

Experimental Section

Materials

Poly(ethylene oxide) (PEO) with an average M_v of 5,000,000 g/mol (Sigma-Aldrich), potassium bis(trifluoromethanesulfonyl)imide (KTFSI, 99.5%, Solvionic), γ-Al_2O_3 nano powder (99.97%, avg. particle size: 20–30 nm, pH 5.0–6.5, Nanostructured & Amorphous Materials, Inc., USA) and SiO_2 nano powder (>99+%, avg. particle size: 20 nm, pH 5.5–6.5, Nanostructured & Amorphous Materials, Inc., USA) were dried at 110 °C for 12 h under vacuum (10^{-3} mbar) prior to use. Carbon black (SuperC, Imerys Graphite & Carbon, Switzerland), poly(vinylidene difluoride) PVdF (HSV900, Arkema), *N*-methyl-2-pyrrolidone (99.5%, Sigma-Aldrich), anhydrous acetonitrile (99.8%, Sigma Aldrich) were used as received.

Potassium metal (98% stored in mineral oil, Sigma-Aldrich) was transferred to the Ar-filled glovebox (H_2O < 0.1 ppm, O_2 < 0.1 ppm), washed with hexane and further used under inert atmosphere.

Solid polymer electrolytes (SPEs) preparation

For the SPE films preparation, 300 mg of dried PEO (6.82 mmol of EO units) and 181 mg of dried KTFSI (0.57 mmol; 37.6 wt.%), corresponding to the molar ratio of ethylene oxide (EO):K = 12:1, PEO_{12}-$KTFSI_1$, and the predefined amounts of dried inorganic nanofiller (Al_2O_3, SiO_2), corresponding to a certain mass fraction (0, 2, 5, 8, 10, 12, 15 wt.% relatively to the polymer-salt composition), were weighed in a ball-mill container. The container was transferred to a ball-mill mixer SPEX 8000, and the components were mixed as dry solids for 1 h. Subsequently, 12 mL of anhydrous acetonitrile was added to the resulting solid mixture, and the slurry was stirred overnight. The solutions were casted onto Teflon molds with an inner diameter of 40 mm, followed by the solvent evaporation at 60 °C. The obtained films were dried at 110 °C for 36 h under vacuum (10^{-3} mbar) and transferred to the Ar-filled glovebox (H_2O < 0.1 ppm, O_2 < 0.1 ppm) without further exposure to air or moisture, where all preparations for following measurements were carried out. The derived films with a thickness of ~200 μm were further used for all measurements.

Characterization of polymer electrolytes

Differential scanning calorimetry (DSC). For DSC measurements, NETZSCH DSC 214 calorimeter was used to register scans in the temperature range from −70 to 160 °C (scan rate of 10 K min^{-1}). When processing the data, the heat flow was normalized by the sample mass. For pristine PEO_{12}-$KTFSI_1$ without nanofiller, the weight fraction of the crystalline phase was calculated relatively to theoretical melting enthalpy of PEO (ΔH_m. = 196.4 J g^{-1}),[45] while for the samples with the nanofillers the total amount of the additives, ϕ_{add}, was accounted according to Equation (1):[46]

$$X_C = \left(\frac{\Delta H_m}{\Delta H(PEO)_m \times (1 - \phi_{add})} \right) \quad (1)$$

Oscillatory rheology. Rheological measurements were performed on a strain-controlled ARES G2 (TA Instruments) rheometer via small amplitude oscillatory shear (SAOS) with shear strains amplitudes γ_0 = 0.1–1%. The tests were conducted on the above prepared SPEs under nitrogen atmosphere in the angular frequency range from 0.1 to 100 rad s^{-1} at 25 °C and 55 °C using an 8 mm parallel plate geometry.

Electrochemical impedance spectroscopy (EIS). Prior to EIS measurements, the coin-type cells (2032-type round button cell) were assembled in an Ar-filled glovebox. To do so, the SPE films with a diameter of 12 mm and a thickness of ~200 μm were sandwiched between two stainless steel electrodes in a coin-type setup. To avoid electrode-electrode contact, gasket rings made from Mylar separators with 100 μm thickness and an inner diameter of 12 mm and external diameter of 16 mm were used. Subsequently, the cells were sealed and pre-conditioned at elevated temperature of 60 °C for 12 h in a temperature chamber, followed by cooling to ambient temperature (25 °C). After another 12 h at 25 °C, EIS measurements were performed on a VSP potentiostat (BioLogic Science Instruments) at the frequency range from 1 MHz to 500 mHz (and reverse) with an amplitude of 20 mV in the temperature range from 15 to 85 °C in 10 °C steps. The temperature ramp rate was 1 °C min^{-1} over 10 min. After each temperature ramp, the temperature was maintained constant for 40 min prior to recording three sets of impedance spectra (ca. every 13 min a new EIS spectrum was recorded). The heating profile was reversed at 85 °C and cooled down to 15 °C under similar conditions.

Further, the bulk electrolyte resistance (R_b) was estimated from the Nyquist plot, and the ionic conductivity (σ) was calculated according to Equation (2):

$$\sigma = \frac{1}{R_b} \cdot \frac{l}{A} \quad (2)$$

where l represents the thickness, and A represents the area of a SPE film.

Cell Assembly and Electrochemical analysis

Electrode preparation. Synthesis of potassium iron hexacyanoferrate, i.e., $K_{2-x}Fe[Fe(CN)_6]$ (KFF) as well as the procedure of electrode preparation were described in detail in our previous studies.[17,18] In brief, KFF was synthesized via co-precipitation of $FeSO_4$ and $K_4Fe(CN)_6$. The composition of KFF was determined by thermogravimetric analysis (TGA) and inductive coupled plasma optical emission spectroscopy (ICP-OES) to $K_{1.90}Fe[Fe(CN)_6]\times1.0H_2O$. Further, active material electrode slurries were prepared, containing 180 mg of KFF, 90.0 mg of carbon black (CB), 30.0 mg of PVdF, 30.0 mg of PEO and 14.0 mg of KTFSI (overall electrode composition 52.3 : 26.2 : 8.7 : 8.7 : 4.1 ratio by mass, wt.%). Electrode coatings were produced by doctor blading and dried subsequently in a climate chamber at 60 °C overnight. The electrode sheets were calendared to a thickness of ~40 μm and cut into discs with a diameter of 16 mm and a mass loading of ~1 mg cm^{-2}. The electrode discs were then dried at 110 °C, respectively, for 12 h under vacuum (10^{-3} mbar) and transferred to an Ar-filled glovebox without further exposure to air or moisture prior to use.

Symmetrical cells assembly. For plating and stripping experiments, symmetrical K/SPE/K coin cells (Hosen CR2032-type cells, SUS316L) were assembled in an Ar-filled glovebox. The SPEs based on PEO_{12}-$KTFSI_1$ with 8 wt.% of the inorganic nanofiller (Al_2O_3 or SiO_2) (further denoted as AlOx-8 and SiOx-8) with a thickness of ~200 μm and a diameter of 16 mm (for AlOx-8) and 14 mm (SiOx-8) were placed between two potassium metal electrodes.

Half cells assembly. Coin cells were assembled in an Ar-filled glovebox from K-metal negative electrodes, KFF positive electrodes and a SPE sandwiched between both electrodes. Specifically, the SPE compositions used in these experiments contained either 8, 10 or 12 wt.% Al_2O_3, 8 wt.% SiO_2 or a mixed composition of 5 wt.% Al_2O_3 and SiO_2 each. The K/SPE/KFF half-cell configurations cycled galvanostatically as described below.

Potassium metal plating and stripping experiments. Potassium metal plating and stripping experiments were conducted in symmetrical cells on a VMP-300 potentiostat (BioLogic Science Instruments) at a temperature of 55 °C. Prior to cycling, the cells were pre-conditioned at OCV at this temperature for 4 h. Then electrochemical impedance spectroscopy (EIS) measurements were performed in 4 h intervals in the frequency range between 10 mHz and 200 kHz and a voltage amplitude of 20 mV. The total conditioning time was 42 h and 13 min. The current densities (j, where $j = I/A$) of 0.01, 0.02, 0.05, 0.075 and 0.1 mA cm^{-2} were used. At j of 0.01, 0.02, 0.05 and 0.075 mA cm^{-2}, each cycle comprised plating and stripping (for 1 h each, for 20 h in total). At 0.1 mA cm^{-2}, the cells were cycled for 200 h in total. When switching from plating to stripping (and reverse), a rest step of 30 min was applied. After each j increase, EIS was conducted under the same conditions as for the OCV phase.

Galvanostatic cycling. Galvanostatic cycling was conducted on a VMP-300 potentiostat (BioLogic Science Instruments) at a temperature of 55 °C. Prior to cycling the cells were conditioned at OCV for 20 h at this temperature. The K/SPE/KFF cells were cycled under constant current constant voltage (CCCV) conditions within the voltage limits of 2.5–4.3 V vs. K^+/K. For the K/SPE/KFF cell with 8-Al_2O_3-PEO_{12}-$KTFSI_1$ SPE, the cycling rate C/25 (1 C = 141 mAh g^{-1} with respect to the theoretical capacity of $K_{1.90}Fe[Fe(CN)_6]\times1.0H_2O$) was used. The cells with 8-, 10-, 12-Al_2O_3-PEO_{12}-$KTFSI_1$, 8-SiO_2-PEO_{12}-$KTFSI_1$, 5-Al_2O_3-5-SiO_2-PEO_{12}-$KTFSI_1$ SPEs, were cycled with a rate of C/15. In the constant voltage (CV) step a current cut-off limit equivalent to C/50 was applied for a maximum of 1 h in both the charge and discharge sequence.

Potentiostat data processing. The galvanostatic cycling data was exported to TXT file extension using the EC-Lab software (V11.27) and further processed using the in-house developed «bat2dat» R package that is available on github.[47]

Results and Discussion

In our previous study,[17] PEO_x-$KTFSI_y$ (with EO:K molar ratio $x:y = 16:1$ and 12 : 1) exhibited the highest room temperature total ionic conductivities (σ of 2.0–3.5×10^{-5} S cm^{-1}) due to their predominantly amorphous nature, low melting points and liquid-like rheological properties. As a result, they are rendered, unsuitable to serve as separators in KIBs configurations. To counteract the mechanical disadvantages of these compositions, composites incorporating nano-sized inorganic fillers, specifically as Al_2O_3 and SiO_2, in a PEO_{12}-$KTFSI_1$ matrix were studied in the first part of this work with respect to their thermal, rheological and ion transport properties. In the second part, the electrochemical tests of selected SPEs will be demonstrated in symmetrical K-K cells and in half cell configurations using K-metal as negative and $K_{2-x}Fe[Fe(CN)_6]$, KFF, as positive electrode.

Physical properties of PEO-based polymer electrolyte composites

Thermal properties. DSC measurements were conducted to evaluate the impact of the nanofillers (Al_2O_3, SiO_2) addition on thermal properties of SPEs based on the PEO-KTFSI composition with EO : K molar ratio = 12 : 1 (Figure S1, summary given in Table 1). Both melting (T_m) and glass transition (T_g) temperatures are plotted in in Figure 1 (T_m refers to the temperature at the peak maximum). It was found that SiO_2-containing composites displayed no dependencies between filler content and T_g, within a margin of ±2 °C, with respect to the pristine PEO_{12}-$KTFSI_1$ composition ($T_g = -45.2$ °C). Marginally higher T_gs are observed for electrolytes with filler contents of 5, 8 and 12 wt.% Al_2O_3, without a clear trend in glass transition temperature. As will be discussed later, differences between the fillers may arise from different degrees of surface-polymer and surface-ion interactions, which can alter the polymer chains dynamics in the electrolytes. As can be seen in DSC scans in Figure S1, the endothermic peaks around the melting temperature comprised of at least two broad overlapping features. Moreover, in the case of AlOx-5, two endothermic peaks were clearly observed, which are both reported in Table 1. In

Research Article
doi.org/10.1002/batt.202300404
Chemistry Europe
European Chemical Societies Publishing

Table 1. Thermal quantities (T_g, T_m, ΔH_m, and mass weighted degree of crystallinity X_C) of pristine PEO_{12}-$KTFSI_1$ (Entry 1) and Al_2O_3/SiO_2-filled PEO_{12}-$KTFSI_1$ samples with different mass fraction of the nanofillers (Entry 2–11).

Sample	Nanofiller	Nanofiller mass fraction [wt.%]	T_g [°C]	T_m [°C]	ΔH_m, [J g^{-1}]	Crystallinity X_C* [%]
PEO_{12}-$KTFSI_1$ (AlOx-0/SiOx-0)	–	0	−45.2	39.9	31.9	16.2
AlOx-2	Al_2O_3	2	−43.5	50.1	47.5	24.7
AlOx-5		5	−38.7	43.2/59.0	54.4	29.2
AlOx-8		8	−41.5	48.8	43.6	24.1
AlOx-10		10	−43.2	56.3	52.7	29.8
AlOx-12		12	−38.1	45.0	40.7	23.5
AlOx-15		15	−42.6	46.6	38.1	22.8
SiOx-2	SiO_2	2	−46.5	45.5	46.1	24.0
SiOx-5		5	−45.4	46.5	42.4	22.7
SiOx-8		8	−43.7	47.7	46.2	25.6
SiOx-10		10	−43.1	51.4	41.4	23.4

*calculated according to Eq. (1), as described in the experimental section.

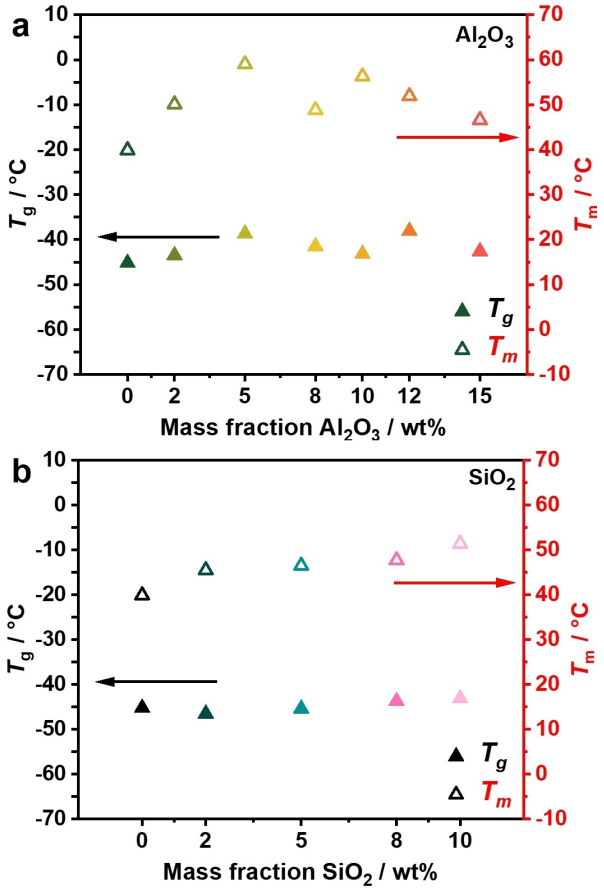

Figure 1. Dependency of the T_g and T_m on the mass fraction of nano-sized a) Al_2O_3 and b) SiO_2 in PEO_{12}-$KTFSI_1$-based SPEs.

composites of SiO_2 (Figure S1b), the endothermic peaks appear to overlap stronger, but still show a discernible shoulder. This suggests the presence of several crystalline phases (with compositional differences), as described previously for PEO-LiTFSI systems.[48,49] By comparison with filler-free PEO_{12}-$KTFSI_1$, one component can be attributed to its melting point at T_m = 39.9 °C, which is a substantial reduction in melting point (from 69 °C for pure, linear PEO at high molecular weight). The melting points of filler-containing samples are clustered around 46.5 ± 2 °C with few compositions exceeding 50 °C. Based on the thermal properties of various PEO_x-$KTFSI_1$ (x = 4,8,12,16,20) compositions from our previous study,[17] the melting points of the adjacent PEO_8-$KTFSI_1$ composition (48.8 °C) and the majority of filler-containing samples tested herein coincide almost. The formation of a crystalline PEO_8:$KTFSI_1$ phase, or more generally segregation into K-rich PEO phase(s) and K-depleted PEO phase(s), as described by Marzantowicz *et al.*[50] for PEO:LiTFSI electrolytes, could explain the mixed phase thermal behaviour. The local immobilization of PEO chains at the nanoparticle surface may induce crystallisation and phase separation, in which the nanofillers act as nuclei or seeds for nucleation and growth and, as a result, melting enthalpies increase (ΔH_m and X_C, respectively, in Table 1).

This contradicts the general hypothesis in related Li- and Na-systems that nanoparticles act as plasticizers in the amorphous regions due to the creation of free volume. Nanoparticles also suppress polymer chain ordering and consequently suppress crystalline growth and larger crystalline regions.[35,37,39] When comparing with literature data, it is worth noting that the impact of ceramic fillers on thermal behaviour of PEO-based electrolytes have been studied mostly in Li^+-containing systems. Compared to Li^+, the larger and softer K-cation[51] is expected to interact weaker with charged surface groups, the polymers' EO units or the salt anions.[52,53] Furthermore, Lee et al.[54] demonstrated that polyester-ZrO_2-LiTFSI composites display different trends in T_g depending on both filler and salt content. In a comparable work Serra Moreno et al.[38] reported decreasing crystallinities of PEO_{20}-$NaTFSI_1$ electrolytes by about 10% and slightly lower melting points upon addition of 5 and 10 wt.% of nano-sized SiO_2, respectively.

Research Article
doi.org/10.1002/batt.202300404
Chemistry Europe
European Chemical Societies Publishing

According to the authors, compositions with higher salt contents showed no significant melting enthalpy (ΔH_m(PEO_{12}-$NaTFSI_1$) $<3.1\ J\,g^{-1}$) and the impact on fillers was not tested in this case.

Rheological characterization. Further, we investigated rheological properties, i.e., mechanical integrity, of the Al_2O_3- and SiO_2-filled PEO_{12}-$KTFSI_1$ electrolytes by small amplitude oscillatory shear (SAOS) tests (Figure 2). Under oscillatory shear, polymer electrolytes generally display viscoelastic behaviour, where the shear storage (G′) modulus represents the viscous portion and the shear loss (G″) modulus expresses the elastic portion of viscoelastic behaviour. When $G' > G''$ is observed, a

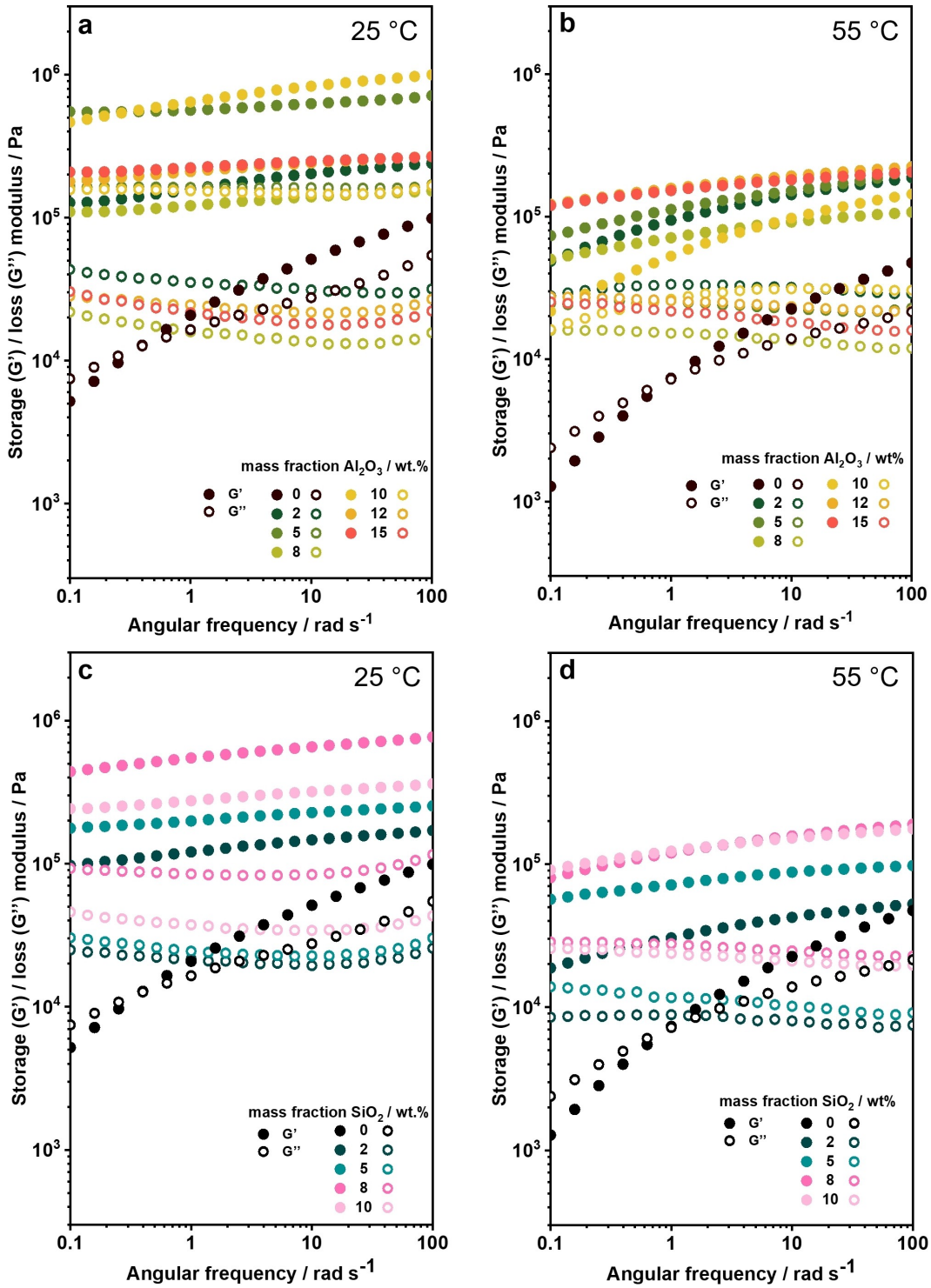

Figure 2. Dependency of storage (*G′*) and loss (*G″*) moduli on angular frequency of PEO_{12}-$KTFSI_1$-based SPEs with different mass fraction of Al_2O_3 at a) 25 °C and b) 55 °C and SiO_2 at c) 25 °C and d) 55 °C. Data for the filler-free PEO_{12}-$KTFSI_1$ was added using the data provided in our previous study.[17,55] Clearly the filler content increases both, the storage and the loss module indicating a transition from a polymer melt to a polymer network.

sample shows solid-like properties, while G'' > G' indicates a liquid-like state.[56] Figure 2(a and b) presents the dependency of the shear moduli (*G'* and *G''*) on angular frequency of the Al_2O_3-filled PEO_{12}-$KTFSI_1$ with different mass fraction of the filler at 25 and 55 °C, respectively. At 25 °C, the filled samples exhibited more than one order of magnitude higher G' as compared to the pristine PEO_{12}-$KTFSI_1$ in the low-frequency region (1.1–5.5×10^5 vs. 5.0×10^3 Pa at 0.1 rad s^{-1}, Figure 2a). Moreover, all modified electrolytes in the investigated range of the filler concentration displayed G' > G'' and display a rubber plateau. This corresponds to the desired solid-like behaviour required for SPEs and also confirms the assumption that crosslinks are introduced by addition of filler. In contrast, the filler-free PEO_{12}-$KTFSI_1$ (black circles) showed an opposite behaviour at small angular frequencies (*G'' > G'*), indicating liquid-like properties. In Figure 2(a), it can also be seen that the two compositions with higher melting point, i.e., AlO*x*-5 and AlO*x*-10, showed a notable shift in higher shear storage and loss moduli (by about half an order of magnitude) over the other investigated samples. As the desired solid-like behaviour (*G' > G''*) was manifested for the SPEs at ambient temperature, we expected to obtain free-standing films for all Al_2O_3-PEO_{12}-$KTFSI_1$ samples in the investigated range of the filler concentration. Contrary, the SPEs containing less than AlO*x*-5 did not yield a good processable, free-standing polymer electrolyte film. At 55 °C (Figure 2b) all compositions surpassed their melting points, which appears to eliminate major differences between the compositions. As seen in Figure 2(b), the largest decrease of storage moduli was shown by the SPEs with AlOx-5 and AlOx-10, ca. one order of magnitude, while the compositions AlO*x*-2 and AlOx-8decreased by ca. half an order of magnitude, and the AlO*x*-12 and AlO*x*-15remained almost unchanged). It should be noted that the corresponding shear loss moduli remain by and large in the same range and, more importantly, do not intercept the storage moduli curves in the measured frequency range (i.e., *G' > G''* still applies). Noteworthy, AlOx-10 exhibited notably close values of *G'* and *G''* at low angular frequency (0.1–1 rad s^{-1}, Figure 2b).

Similar rheological behaviour was observed for the SiO_2-filled PEO_{12}-$KTFSI_1$ electrolytes (Figure 2c and d). At 25 °C, the storage moduli of the samples with SiO_2 were found in the range of *G'* = 9.4×10^4–4.4×10^5 Pa at 0.1 rad s^{-1}, which is more than one order of magnitude higher compared to G' of the pristine PEO_{12}-$KTFSI_1$ (measured at low angular frequencies). Furthermore, the SiO_2-filled electrolytes manifested solid-like properties (G' > G''), that were preserved at elevated temperature of 55 °C (Figure 2d), although overall the storage moduli decreased, as well as the gap between the storage and loss moduli.

Although the SiO_2-SPEs (with 2–10 wt.% of the nanofiller) displayed viscoelastic solid-like rheological behaviour at 25 °C (Figure 2c). However, in practice free-standing films from SiOx-2 and SiOx-5 could not be obtained, which is a prerequisite for SPE application in K-metal batteries.

The results demonstrate that mechanical properties of PEO_{12}-$KTFSI_1$ compositions can be greatly improved by incorporating Al_2O_3 or SiO_2 inorganic nanoparticles into predominantly amorphous polymer matrix (Table 1). Compared to our previously reported block copolymer electrolyte, the rheological properties show a stronger dependence on temperature.[18]

Ionic conductivities. Next, we conducted EIS in the frequency range from 1 MHz to 500 mHz in a temperature range from 15 to 85 °C (in 10 °C steps) to evaluate the impact of the Al_2O_3 and SiO_2 addition on the total ionic conductivities (σ) of the resulting SPEs (Figure 3a and b). The bulk electrolyte resistance required for Equation (2) was determined from fitting the acquired EIS spectra to a Debye circuit,[57] demonstrated in the example provided in Figure S2 and Table S1. Raw data and corresponding sample thicknesses are provided in the data repository associated with this work.[58] It was observed that both fillers caused no change or even a small reduction in total ionic conductivity with respect to the filler-free PEO_{12}-$KTFSI_1$ (Figure 3a and b) at temperatures above T_m. Compared to filler-free PEO_{12}-$KTFSI_1$ (1.5–3.0×10^{-6} vs. 2.0×10^{-5} S cm^{-1} at 25 °C) the samples containing Al_2O_3 (Figure 3c) or SiO_2 (Figure 3d) showed one order of magnitude lower σ. When the temperature approached 45 °C (close to T_m of the filled SPEs, see Table 1), the difference in ionic conductivities became negligible (the same order of magnitude for the filler-free and modified PEO_{12}-$KTFSI_1$, around 1.0×10^{-4} S cm^{-1}). Upon further increase of the experimental temperature, the σ deviation remains the same (55–85 °C, Figure 3a). At 55 °C, the samples demonstrated σ of 1.4–2.6×10^{-4} S cm^{-1}. For comparison, similar ionic conductivities were measured previously for PEO_{20}-$KTFSI_1$ (2.8×10^{-4} S cm^{-1}).[17] Similar findings of the ion transport dependency on temperature were manifested for the SiO_2-containing PEO_{12}-$KTFSI_1$ samples.

The ionic conductivities obtained for the SiO_2/Al_2O_3-containing PEO_{12}-$KTFSI_1$ electrolytes are in a similar range as in the work by Serra Moreno et al.[38] on the corresponding nano-SiO_2-PEO_{20}-$NaTFSI_1$ compositions. As for the samples studied herein, the authors found that the ionic conductivity were not affected significantly by the filler content (i.e., 5 and 10 wt.% of SiO_2). However, in their case, the ionic conductivities followed closely the ones of a filler-free sample even below the melting point. By far most results were reported for composites based on PEO:LiTFSI. For example, Jayathilaka et al. reported[59] room temperature ionic conductivities of up to 0.22 mS cm^{-1} for a $PEO_9LiTFSI_1$ composite with 10 wt.% porous Al_2O_3 (104 μm particle size; 155 m^2 g^{-1}). Similar values were reported in a recent study by Yang et al.[60] for SiO_2 (7–40 nm) composites ($PEO_{15}LiTFSI_1$). This is largely in agreement with previous conductivity comparisons[18,61] between the monovalent cations Li^+, Na^+ and K^+, where PEO-based electrolytes with ATFSI (A = Li, Na, K) salts also displayed similar ionic conductivities, independent of the cation (an increase in transference number for larger cations could be shown by Oteo et al.[61]).

Discussion. The following section provides a discussion on the structure-property relationships in the studied PEO_{12}-$KTFSI_1$ composites in the context of previous works on the impact of inorganic fillers on the polymer electrolyte properties.

(1) In literature, the effect of ceramic fillers beyond reported improvements of mechanical properties is controversially discussed.[38,62] For Li-SPEs, ceramic fillers were studied in a

Research Article
doi.org/10.1002/batt.202300404
Chemistry Europe
European Chemical Societies Publishing

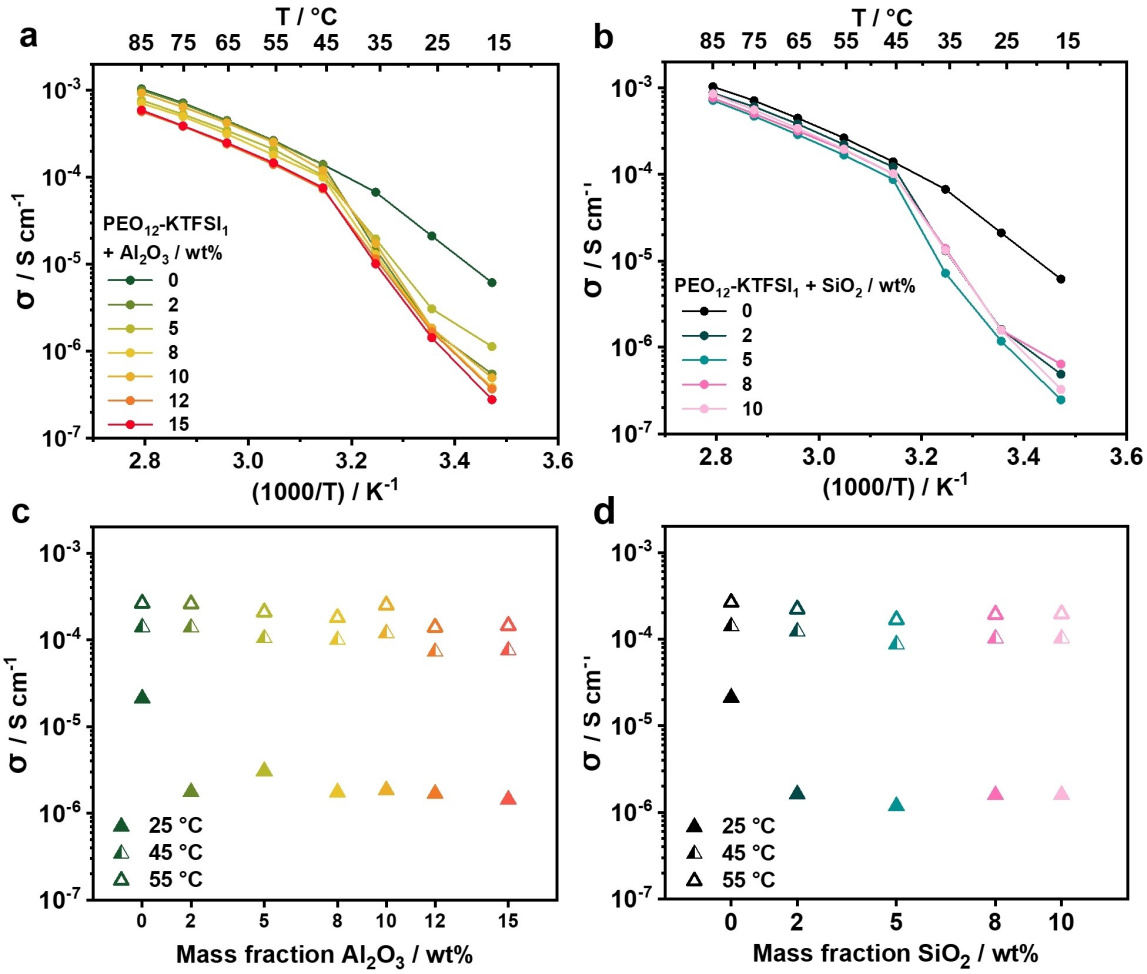

Figure 3. Temperature-dependent ionic conductivity (derived from EIS conducted in the frequency range from 1 MHz to 500 mHz) of PEO_{12}-$KTFSI_1$-based SPEs with different mass fraction of a) Al_2O_3 and b) SiO_2. Dependency of ionic conductivity in PEO_{12}-$KTFSI_1$-based SPEs on mass fraction of c) Al_2O_3 and d) SiO_2 at 25, 45 and 55 °C.

variety of different electrolyte salts for PEO-LiX composite electrolytes (X = BETI,[62,63] TFSI[59,60,64] or triflate ($SO_3CF_3^-$)[39]). The composition with an EO:Li molar ratio of 20:1 seemed particularly favoured, which is interesting from the perspective of its high degree of crystallinity of over 50%.[65] In those cases, addition of fillers indeed reduced the crystalline phase. However, the effect of ceramic fillers appears to diminish when formulations with low crystallinity are used as starting formulation (for $PEO_{12}KTFSI_1$ $X_C = 16\%$). Further improvements in ion conduction, then depends on other effects, like facilitated ion transport at the particle interface or anion immobilization (higher transference numbers). However, both dielectric spectroscopy[59] and NMR spectroscopy[62] studies found merely modest improvements in ion mobility by addition of ceramic fillers, as diffusion and relaxation activation energies are reduced.

(2) Lewis acid-base interactions between the ceramic particle surface and the ion-conducting salt can facilitate salt dissociation. However, the dissociation energies of NaTFSI and KTFSI are lower than that of LiTFSI (~590 kJ mol^{-1} (LiTFSI), ~490 kJ mol^{-1} (NaTFSI) and ~425 kJ mol^{-1} (KTFSI)).[66] Therefore, the benefit may dissipate with decreasing dissociation energies.

(3) The degree of interactions between $TFSI^-$ anions and PEO chains with the ceramic surface strongly depends on the nature of the surface groups.[39] Lewis acidic surface groups may interact with both anions and EO ether fragments. This may lead to formation of Li^+-conduction pathways along the particle interface. While little or no interactions are expected between anions and Lewis basic surface groups, Croce et al. also postulated surface-Li^+-PEO interactions with Li^+ as a mediator *via* electrical ion-dipole interactions.[39] The latter may come at the expense of Li^+ immobilization. In their work, the authors presented evidence that ion transport is indeed higher for acidic or neutral (amphoteric) particle surfaces but similar to the filler-free material for basic particle surfaces. Based on the supplier data, the nanoparticles used for this study exhibited slightly acidic surfaces (pH between 5.0–6.5), although their isoelectric points are notably different (Al_2O_3 ~pH 9; SiO_2 ~pH 2).[67] The latter may affect the dispersion properties of the particles. Further, it should be acknowl-

Research Article
doi.org/10.1002/batt.202300404
Chemistry Europe
European Chemical Societies Publishing

edged that cation-surface interactions could be smaller with a soft Lewis-acid like K^+, which might reduce the impact of this effect on ion mobility for K^+-conductors.

(4) Nanofiller-PEO and nanofiller-salt interactions can result in structural reorganisation of polymer chains around the particles that can promote crystal growth through immobilization of polymer segments in proximity to the particle interface. As discussed in the section on the thermal properties above, addition of either Al_2O_3 or SiO_2 fillers to PEO_{12}-$KTFSI_1$-lead to higher degrees of crystallinities between 6–13 wt.% with respect to the filler-free composition ($X_C = 16.2$ wt.%). Higher degrees of crystallinity and the possibility of particle crosslinking through the polymer phase improved the mechanical properties of composite films and restored viscoelastic behaviour in the PEO_{12}-$KTFSI_1$ composition. On the other hand, the overall ion transport properties are likely adversely affected in presence of more crystalline domains and locally restricted chain motion, since ion transport occurs predominantly in the amorphous phase. Hence, as the crystalline domains dissolve above T_m the ionic conductivities of filler-containing samples approach similar values as the filler-free PEO_{12}-$KTFSI_1$ formulation. Conversely, below T_m ion transport is hindered in samples with nanofillers.

(5) The degree of interactions is coupled to the particle size of the filler, which should be below 1 μm to achieve improved ionic conductivities.[38,68] The previous work[39] discussed above, used SiO_2 particle sizes as low as 5–7 nm. Even in this case ionic conductivities of SiO_2-PEO_{20}-NaTFSI composites did not surpass that of the filler-free PEO_{20}-NaTFSI formulation. With particle sizes of around 30 nm for both Al_2O_3 and SiO_2 (see Experimental Section), the ceramic fillers used herein are on the smaller end of the scale, but the degree of interactions could be further increased through even smaller particles.

Electrochemical characterization

Symmetrical cell tests. As mentioned in the rheology section of this study, in practice some samples did not yield processable free-standing films. Therefore, we chose the compositions containing 8 wt.% of filler (AlOx-8 and SiOx-8) for a first evaluation of cell resistances in plating and stripping experiments in symmetrical K/SPE/K cells at 55 °C, shown for both composites in Figure 4(a) and (b), respectively. To do so, the cells were cycled at gradually increasing current densities *j* of

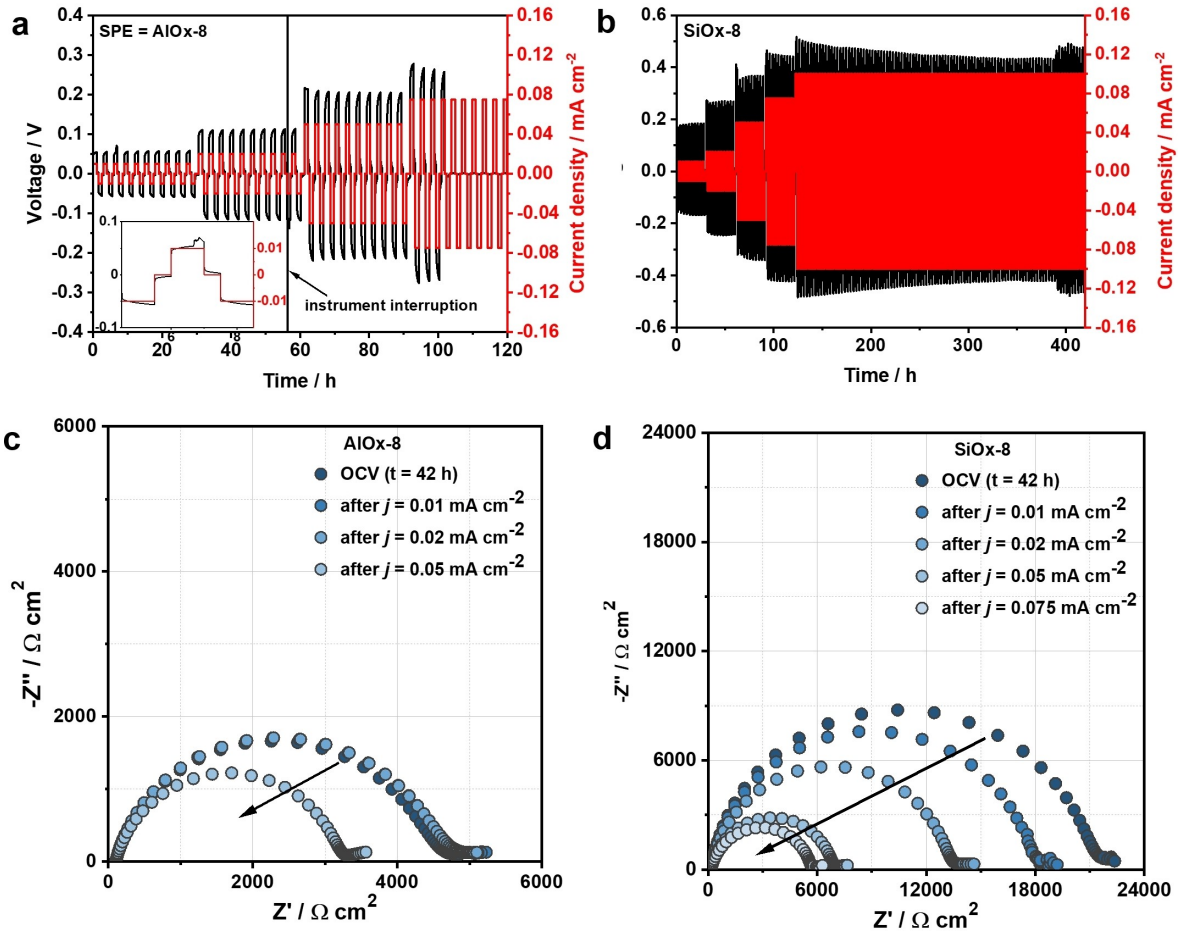

Figure 4. Plating/stripping experiments in symmetrical K/SPE/K cells at 55 °C with current densities (*j*) of 0.01, 0.02, 0.05, 0.075 and 0.1 mA cm^{-2} where SPE = a) AlO*x*-8, b) SiOx-8. EIS conducted in the frequency range from 200 kHz to 10 mHz after every *j* increase in K/SPE/K cells where SPE = c) AlO*x*-8, d) SiOx-8.

0.01, 0.02, 0.05, 0.075 and 0.1 mA cm^{-2} and a sequence duration of 1 h and a 30 min OCV relaxation step.

As seen in Figure 4(a), the symmetrical K-cell with AlOx-8 SPE demonstrated a reversible metal deposition at *j* of 0.01, 0.02, 0.05 mA cm^{-2}. At the lowest current density, i.e., $j=$ 0.01 mA cm^{-2}, the cell showed overpotentials of ~60 mV. In the 3rd cycle, voltage fluctuations were observed (see inset in Figure 4a), possibly associated with surface processes.[69] At higher *j* of 0.02 mA cm^{-2}, overpotentials increased almost doubled and corresponded to ~110 mV. At $j=0.05$ mA cm^{-2} our K/AlOx-8/K cell enabled cell cycling only under substantial overpotential of $\leq$220 mV. Thus, in first approximation, the plating and stripping overpotentials scale linearly with *j*. Further, a short circuit occurred in the following sequence at 0.075 mA cm^{-2}. This is associated most likely, with K-metal dendrite growth, adversary affecting the cell performance in plating and stripping experiments.[25,70]

For K/SiO*x*-8/K cell (Figure 4b), notably higher overpotentials were observed when plating and stripping at the same current densities as in the case of symmetrical cell with AlO*x*-8. Thus, overpotentials of ~180 mV corresponded to $j=$ 0.01 mA cm^{-2}, followed by increase to ~260 mV at 0.02 mA cm^{-2}, and further to ~360 mV at 0.05 mA cm^{-2}. Contrary to the AlOx-8 electrolyte, neither fluctuating voltages nor short circuit were noted. Moreover, the cell with SiO_2-filled sample completed the sequence at 0.075 mA cm^{-2} with initial overpotentials of ~520 mV. The overpotential decreased with increasing number of cycles to 430 mV, which is still quite substantial. Overall, the cell could be operated for over 250 h at a current density of 0.1 mA cm^{-2} and thus showed considerably better cycling stability than the Al_2O_3 composite.

For comparison, under the same experimental conditions symmetrical cells employing poly(vinyl benzyl methoxy poly(ethylene oxide) ether)-*block*-polystyrene block copolymer and KTFSI, reported in our previous work,[18] displayed overpotentials of 330 mV at 0.05 mA cm^{-2}, which is in the same range as the SiO_2 composite but about 110 mV higher than the Al_2O_3 studied herein. However, analogous symmetrical Li-cells demonstrated ca. 10 times lower overpotentials at given current densities. Higher overpotentials in the case of K-metal are attributed to larger cell resistance, due to formation of a resistive surface layer, i.e., SEI layer.[71]

For this reason, electrochemical impedance spectroscopy (EIS) spectra were recorded at the end of each cycling segment, i.e., before the next higher current density was applied. Figure 4 shows the evolution of the cell impedance after every 10 cycles (each cycling segment) for AlO*x*-8 (Figure 4c) and SiO*x*-8 (Figure 4d).

At least two discernible processes with different time constants contributed to the impedance spectrum before plating and stripping, while different electrode processes in the spectra of the cycled cells could not be properly distinguished. Considering a high reactivity of potassium, contributions of both the charge-transfer reaction and the surface layer were expected.[71] In addition, the electrolyte resistance and a dielectric contribution from the polymer electrolyte might add to the frequency arcs that may be interpreted as a single electrode process, i.e., a single semicircle. Comparing the diameter of the frequency arcs (using data points at the same frequency), it is seen that the impedance in the system decreased with increasing current density. This finding is in contrast with the expectation that a reactive K-metal electrode should show increasing impedance as cycling (and thus aging) progresses. This is an indication, however, that the plating and stripping process removes some of the charge-transfer inhibiting compounds from the surface (or fresh K-metal is plated on the surface). Moreover, increase of the electrode surface, e.g., by growth of dendrites or formation of more porous morphologies may reduce the impedance that is normalized to the geometric electrode area. At the same time, based on the EIS results, the SEI layer growth does not appear to be critical at this stage of the cycling process (but might become more significant as the cell ages).

Evidently, SiO_2-based polymer electrolytes showed higher areal resistance (by a factor of 5) compared to Al_2O_3 composites at the beginning of the first cycling sequence. Interestingly, over the course of 30 cycles at three different current densities, the impedance of the cell containing SiOx-8 decreased considerably and approached similar values than the cell containing AlOx-8. Although the impedances equilibrate to similar values, the overpotentials during cycling remained larger for the SiO_2 composite, indicating that practically K^+-ion transport is slower (higher polarization) in this formulation.

Galvanostatic cycling in 2-electrode half cell configurations. Lastly, the SPEs based on PEO_{12}-$KTFSI_1$ with Al_2O_3 and SiO_2 nanofillers were tested in potassium half cells, comprising $K_{2-x}Fe[Fe(CN)_6]$, KFF, as the positive electrode and K-metal as negative electrode. The chemical composition of KFF was calculated to $K_{1.90}Fe[Fe(CN)_6]\times1.0H_2O$, corresponding to a theoretical capacity of 141 mAh g^{-1}. In our previous work a specific capacity of 120 mAh g^{-1} was achieved with this electrode material.[18]

For galvanostatic cycling tests of Al_2O_3-SPEs, three compositions were chosen with 8, 10 (AlO*x*-8 and AlO*x*-10), and 12 wt.% (AlO*x*-12) of nano-Al_2O_3, respectively. The cells were cycled at a C-rate of C/15 with a voltage window of 2.5–4.3 V vs. K^+/K at elevated temperature of 55 °C. Capacity retentions and corresponding coulombic efficiencies (C.E.) are provided in Figure 5(a–c). The voltage profiles for selected cycles are found in Figures S3(b–d). Cycling at temperatures close to ambient temperature, i.e., 25 °C, has been and still is a major bottleneck for SPEs due to their modest ionic conductivities. For Li- and Na-cells, Mindemark *et al.* previously reported polyester-polycarbonate (PCL-PTMC) copolymers that enabled operation at temperatures as low as 40 °C.[72,73] Herein, we present another encouraging example of polymer-based K-ion conductors that approach near-ambient operating temperatures. The AlOx-8 sample (cell 1) was also cycled at 45 °C at a reduced C-rate of C/25 (Figure 5a) The cells show two voltage plateaus of the two characteristic redox steps of KFF upon reduction around 4.05 V and 3.4 V vs. K^+/K (Figure S3a).[13,74] In addition, an intermediate feature is seen between the two plateaus in the voltage range between 3.4–3.6 V vs. K^+/K. In accordance with previous results,[17] the voltage profile is different from those in liquid

Research Article
doi.org/10.1002/batt.202300404
Chemistry Europe
European Chemical Societies Publishing

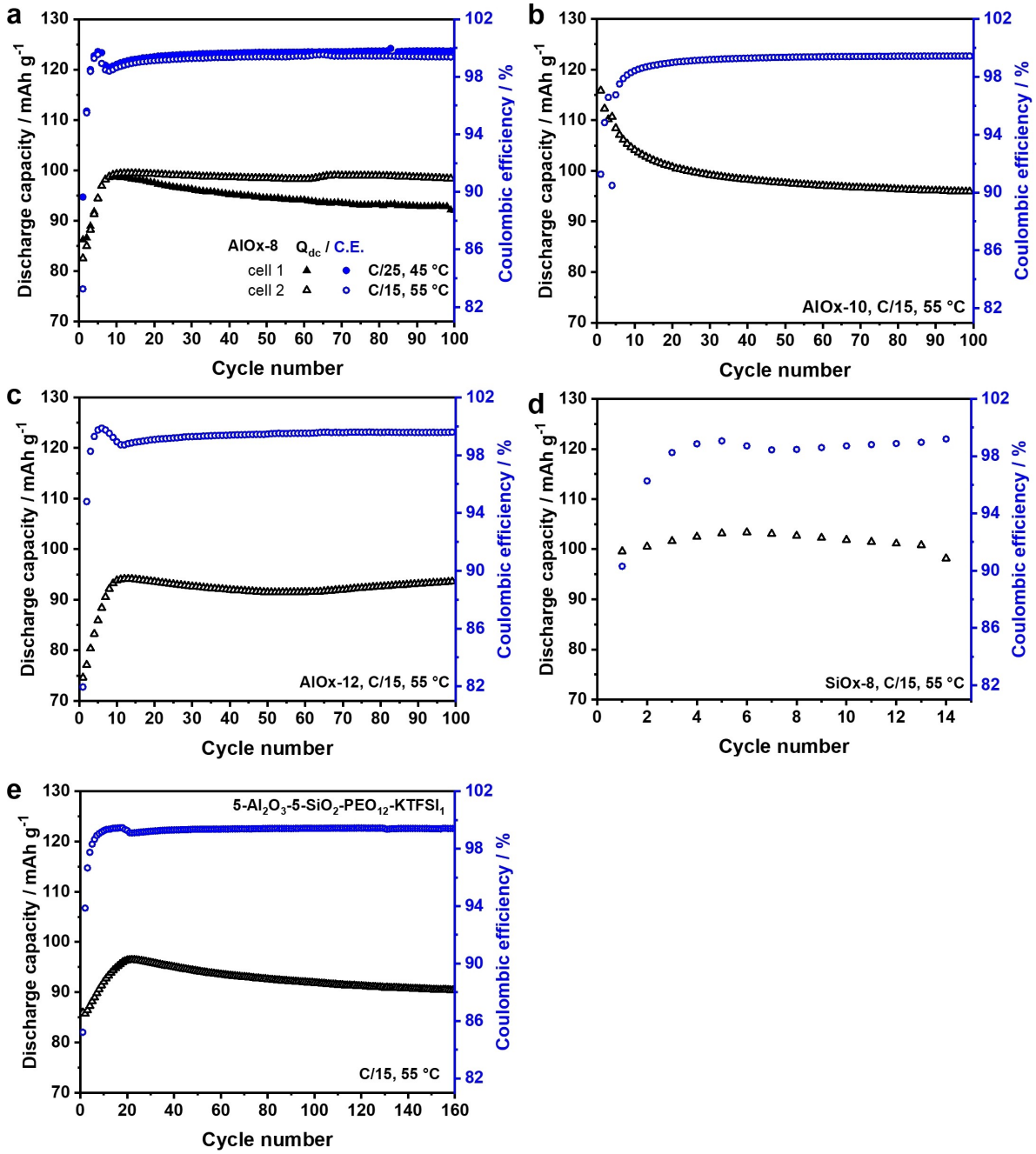

Figure 5. Capacity retention and corresponding coulombic efficiencies of K-metal/SPE/KFF cells employing different SPE composites. For the formulation a) AlO*x*-8 two cells were tested with different current densities. At a slower rate of C/25 the cell showed a continuous capacity loss over the first 100 cycles. The formulations b) AlO*x*-10 and c) AlO*x*-12 were examined at C/15, showing distinctly different capacity loss profiles. The composite d) SiO*x*-8failed after 14 cycles. The overall best performance was obtained from a blend comprising 5 wt.% of Al_2O_3 and e) 5 wt.% of SiO_2.

electrolytes in this respect, as usually a direct drop (or increase) from one plateau to the other is observed. There were no SPE-composition related differences in the shape of the voltage profiles, other than differences in specific capacity (Figure 3a–d).

On the first cycle a comparatively small discharge capacity (Q_{disch}) of 86.2 mAh g^{-1} (C.E. of 89.6%) was obtained (practical capacity of KFF ~120 mAh g^{-1}). A notable increase of Q_{disch} was observed to a maximum of 98.7 mAh g^{-1} delivered in the 10th cycle. This behaviour is well-known for solid-state systems, where the interfacial contact between SPE and active material improves over time and has been observed in our previous work as well as by others.[17,20,75] In order to maintain comparability between the cells herein and our previous work,[17,18] we have maintained the electrode formulation that includes 11.7 wt.% of polymer electrolyte (without filler) and the conditioning time at OCV prior to cycling. To minimize the

initial increase until a maximum capacity is reached these parameters could be further optimized.

Moreover, from the symmetrical cell tests decreasing impedance with increasing cycle number was observed (Figure 4c), which could play a role in the accessible capacity of the two-electrode setup. This conditioning phase is accompanied by a peak in CE that surpasses 100%, as during cycling former inactive active material domains gradually become active. Beyond the 10th cycle, discharge capacity of cell 1 steadily declined, to around 92 mAh g^{-1} after 100 cycles. The observed capacity loss is associated most likely with higher degree of irreversible side reactions at low cycling rates (C/25), that are adversary affecting the long-term capacity retention of the cell. The CE increased from around 99% in the 10th cycle and approached 99.8% CE after 100 cycles. For comparison, in our previous work on filler-free PEO-KTFSI compositions,[17] the C.E. approached values of 98% only slowly over the first 50 cycles, indicating that the addition of filler improved the C.E. significantly.

To promote ion mobility in the AlO*x*-8 and reduce kinetic limitations, a higher cycling temperature of 55 °C and a C-rate of C/15 were used in the following (Figures S3b, 5a, cell 2). Compared to the cell 1 (cycled at C/25 and 45 °C), slightly lower Q_{disch} was measured on the 1st cycle (82.5 mAh g^{-1}), but by the 8th cycle both cells approached similar discharge capacities. As seen in Figure 5(a), cell 2 demonstrated a slight capacity decline over 60 cycles (from 99.4 to 98.2 mAh g^{-1}, ~1%), followed by a recovery back to 99.0 mAh g^{-1}. This could be associated with electrode-electrolyte contact changes over time.[20] Upon further cycling, the cell 2 reached a notably improved capacity retention over the first 100 cycles. Specifically, with respect to Q_{disch} on the 10th cycle, the capacity loss on following cycles was less than 1% until the 100th cycle. We ascribe the better capacity retention to shorter times in the high potential region, as PEO reaches its stability limit in the voltage region between 4.1 to 4.3 V vs. K^+/K.[26,27]

The cell with AlO*x*-12 SPE showed a similar behaviour to that employing AlO*x*-8, i.e., increasing capacities in the conditioning phase in combination with a peak in CE after a few cycles (Figure 5c). The maximum Q_{disch} of 94.1 mAh g^{-1} was obtained on the 13th cycle, and the corresponding CE was between 99.0 to 99.6% until the 100th cycle. The capacity dropped between the 13th and 50th cycle by ca. 3% before it started to increase slightly again. As a result, the capacity retention was 99% after 100 cycles. It is worth noting that both AlOx-8 and AlOx-12 showed reversible discharge capacities around 100 mAh g^{-1}, while somewhat higher initial specific discharge capacity of 115 mAh g^{-1} were previously found in reference measurements with a liquid electrolyte.[17]

Contrary to the previously observed tendency of increasing initial discharge capacities in the conditioning phase, the AlOx-10 cell showed its maximum Q_{disch} of 115.9 mAh g^{-1} on the 1st cycle (Figure 5b), which is in the same range as for a corresponding liquid electrolyte cell.[17] A continuous capacity decay was observed, that was most pronounced from the 1st to 20th cycle and resulting in total capacity retention of 83% after 100 cycles. The initial CE of 91.3% increased to above 99.0% after 20th cycle and reached 99.4% after 100 cycles. In the series of Al_2O_3-composition SPEs AlO*x*-10 was an exception. However, this not only applies to the electrochemical test but is also in agreement with its thermal and rheological properties, where this composition appeared to deviate from other compositions. Its rheological properties for instance ($G' \approx G''$ at small angular frequencies; Figure 2b), could potentially facilitate the SPE penetration into the cathode coating layer.

Further, the PEO_{12}-$KTFSI_1$ SPE employing 8 wt.% of SiO_2 nanofillers was tested in the same cell configuration (K-metal/SPE/KFF) at 55 °C using a C-rate of C/15 with a voltage window of 2.5–4.3 V vs. K^+/K (Figure S3e). As seen in the voltage profiles in Figure S3(e), the cell only enabled 13 cycles before showing voltage noise in the 14th cycle, which in our experience marked the onset of cell failure. The effect of voltage fluctuations during charge/discharge process is often observed for the PEO-based SPEs in lithium metal cells[69,70] and was previously attributed to metallic dendrite growth.[25] As presented in Figure 5(d), the cell achieved 4 mAh g^{-1} higher Q_{disch} maximum compared to the analogous K-metal/SPE/KFF cell with 8 wt.% of Al_2O_3 (Figure 5a, cell 2).

Therefore, we further tested a «hybrid» PEO_{12}-$KTFSI_1$ SPE filled with 5 wt.% Al_2O_3 and SiO_2 each (i.e., 10 wt.% of the nanofillers in total), attempting to merge a stable long-term cycling and a higher capacity (Figure S3f). Capacity retention and corresponding coulombic efficiencies of the cell employing the «hybrid» SPE are shown in Figure 5(e). On the 1st cycle, the cell demonstrated a modest Q_{disch} of 86.0 mAh g^{-1} that drastically increased over the conditioning phase, resulting in the maximum of 96.4 mAh g^{-1} in the 20th cycle. Corresponding CE in the first cycles drastically increased from 85.2 to 99.2% (from the 1st to 20th cycle, respectively) possibly due to the improvement of electrode-electrolyte interface. After reaching the maximum Q_{disch}, the cell exhibited slight but continuous capacity decay, eventually showing capacity retention of 95% after 100 cycles, and 94% after 160 cycles. Furthermore, the cell with this «hybrid» formulation quickly approached CEs >99% (featuring 99.4% CE at the 160th cycle) and displayed the best long-term cycling behaviour.

Conclusions

In this work, Al_2O_3 and SiO_2 nanoparticles in the particle size range between 20–30 nm were incorporated into a PEO_{12}-$KTFSI_1$ polymer electrolyte formulation in mass fractions between 2 to 15 wt.%, with the aim to improve mechanical properties and ion mobility. The ceramic-filler containing formulations showed similar glass transition temperatures but increased melting points, along with crystallinity degrees compared to the filler-free sample. While higher T_ms and crystallinity benefitted the mechanical properties, the ion conduction below T_m showed stronger temperature dependence. Above the melting point at around 45 °C the ionic conductivities of ceramic-containing and ceramic-free samples approached similar values in the range of 1.0×10^{-4} S cm^{-1}. The thermal properties and ion mobility are largely in agreement with the work of Serra Moreno et al.[38] on

PEO_x-$NaTFSI_y$-based composites. However, the addition of ceramic fillers turned the liquid-like filler-free polymer electrolyte back into a viscoelastic, processable and free-standing film, with sufficient mechanical stability at elevated temperatures.

SPEs with filler contents of more than 8 wt.% were examined in symmetrical cell setups and in K-metal/SPE/KFF cell configurations. Plating and stripping experiments showed large impedance, presumably from the interfacial resistance at the electrode-electrolyte interface, for both Al_2O_3- and SiO_2-filled PEO_{12}-$KTFSI_1$ electrolytes. Interestingly, the impedance decreased in later sequences with higher current densities, suggesting that the interfacial resistance decreased. This could be the case, when K-metal is plated on top of a resistive layer, when the porosity increases, and when the electrode-electrolyte contact improves over time. The Al_2O_3-containing sample failed at higher current densities, but conversely performed better than the SiO_2-containing SPEs in the half cell tests.

In the latter experiments, SPEs comprising Al_2O_3 fillers enabled cycling at 45 °C at a C-rate of C/25, and a capacity retention of 93% after 100 cycles. When increasing the temperature to 55 °C the cycling rate could be raised to C/15. After initial conditioning cycles the capacity retention was above 99% on the 100th cycle, despite a higher cycling temperature that may cause more parasitic reactions. In contrast, SiO_2-SPEs enabled slightly higher discharge capacities compared to analogous Al_2O_3-SPEs (4 mAh g^{-1}), however, only short-term cycling was possible before the cells showed initial signs of failure. In attempts to merge a high discharge capacity and superior capacity retention, we further tested a «hybrid» composition comprising both Al_2O_3 and SiO_2 nanofillers. Although the cell showed modest discharge capacities of around 90 mAh g^{-1}, the best long-term cycling behaviour was obtained with a capacity retention of 94% after 160 cycles. Overall, the ceramic-fillers improved capacity retention and allowed cycling over up to 160 cycles after an initial conditioning period and produced similar encouraging cell test results as our previously reported block copolymer approach. In both cases the performance, in terms of capacity retention and coulombic efficiency, was improved over filler-free PEO-KTFSI compositions. Moreover, the ceramic-fillers allow cell cycling under near-ambient (45 °C) conditions, although at low cycling rates, which is an improvement to PEO-based electrolytes in Li-ion systems that typically require temperatures beyond 60 °C.

Acknowledgements

The authors thank Andreas Heyn and Celine Röder for their support with X-ray diffraction measurements. Financial support from the German Federal Ministry of Education and Research (BMBF) within «FestBatt» (13XP0175 C) and the Helmholtz Association is gratefully acknowledged. This work contributes to the research performed within the Post Lithium Storage Cluster of Excellence (POLiS), funded by the Deutsche Forschungsgemeinschaft (DFG, German Research Foundation) under Germany's Excellence Strategy – EXC 2154 – Project number 390874152, as well as to the research performed at the Center for Electrochemical Energy Storage Ulm-Karlsruhe (CELEST). M.H. gratefully acknowledges the support from the Stiftung der deutschen Wirtschaft (sdw) within the Klaus Murmann fellowship for her Ph.D. Open Access funding enabled and organized by Projekt DEAL.

Conflict of Interests

The authors declare no conflict of interest.

Data Availability Statement

The authors declare no competing interests. The data to the above presented findings are available on Zenodo online repository DOI: 10.5281/zenodo.7418421 (ref. [58]). The R package used for processing galvanostatic cycling data is available on github (ref. [76]).

Keywords: solid polymer electrolyte · SPE · inorganic filler · mechanical integrity · potassium-ion battery · KIB · Prussian blue analogue · PBA

[1] B. John, V. Anoopkumar, T. D. Mercy, *ACS Appl. Energ. Mater.* **2020**, *3*, 9478–9492.
[2] T. Hosaka, K. Kubota, A. S. Hameed, S. Komaba, *Chem. Rev.* **2020**, *120*, 6358–6466.
[3] R. Rajagopalan, Y. Tang, X. Ji, C. Jia, H. Wang, R. Rajagopalan, Y. Tang, X. Ji, H. Wang, C. Jia, *Adv. Funct. Mater.* **2020**, *30*, 1909486.
[4] S. Komaba, T. Hasegawa, M. Dahbi, K. Kubota, *Electrochem. Commun.* **2015**, *60*, 172–175.
[5] L. Qiao, X. Judez, T. Rojo, M. Armand, H. Zhang, *J. Electrochem. Soc.* **2020**, *167*, 070534.
[6] A. Hofmann, F. Müller, S. Schöner, F. Jeschull, *Batteries & Supercaps* **2023**, DOI 10.1002/batt.202300325.
[7] F. Allgayer, J. Maibach, F. Jeschull, *ACS Appl. Energ. Mater.* **2022**, *5*, 1136–1148.
[8] L. Madec, V. Gabaudan, G. Gachot, L. Stievano, L. Monconduit, H. Martinez, *ACS Appl. Mater. Interfaces* **2018**, *10*, 34116–34122.
[9] L. Caracciolo, L. Madec, H. Martinez, *ACS Appl. Energ. Mater.* **2021**, *4*, 11693–11699.
[10] F. Jeschull, J. Maibach, *Electrochem. Commun.* **2020**, *121*, 106874.
[11] Badre Larhrib and Lénaïc Madec, *Batteries & Supercaps* **2023**, *6*, 1–23.
[12] Z. Jian, W. Luo, X. Ji, *J. Am. Chem. Soc.* **2015**, *137*, 11566–11569.
[13] X. Bie, K. Kubota, T. Hosaka, K. Chihara, S. Komaba, *J. Mater. Chem. A* **2017**, *5*, 4325–4330.
[14] K. Hurlbutt, S. Wheeler, I. Capone, M. Pasta, *Joule* **2018**, *2*, 1950–1960.
[15] P. A. Morozova, I. A. Trussov, D. P. Rupasov, V. A. Nikitina, A. M. Abakumov, S. S. Fedotov, *Crystals* **2021**, *11*, 895.
[16] M. Fiore, S. Wheeler, K. Hurlbutt, I. Capone, J. Fawdon, R. Ruffo, M. Pasta, *Chem. Mater.* **2020**, *32*, 7653–7661.
[17] A. D. Khudyshkina, P. A. Morozova, A. J. Butzelaar, M. Hoffmann, M. Wilhelm, P. Theato, S. S. Fedotov, F. Jeschull, *ACS Appl. Polym. Mater.* **2022**, *4*, 2734–2746.
[18] A. D. Khudyshkina, A. J. Butzelaar, Y. Guo, M. Hoffmann, T. Bergfeldt, M. Schaller, S. Indris, M. Wilhelm, P. Théato, F. Jeschull, *Electrochim. Acta* **2023**, *454*, 142421.
[19] S. Trano, F. Corsini, G. Pascuzzi, E. Giove, L. Fagiolari, J. Amici, C. Francia, S. Turri, S. Bodoardo, G. Griffini, F. Bella, *ChemSusChem* **2022**, *15*, DOI 10.1002/cssc.202200294.
[20] H. Fei, Y. Liu, Y. An, X. Xu, J. Zhang, B. Xi, S. Xiong, J. Feng, *J. Power Sources* **2019**, *433*, 226697.
[21] H. Fei, Y. Liu, Y. An, X. Xu, G. Zeng, Y. Tian, L. Ci, B. Xi, S. Xiong, J. Feng, *J. Power Sources* **2018**, *399*, 294–298.

[22] L. Qiao, X. Judez, T. Rojo, M. Armand, H. Zhang, *J. Electrochem. Soc.* **2020**, *167*, 070534.
[23] M. Schulz, M. Schäfer, K. Saalwächter, T. Thurn-Albrecht, *Nat. Commun.* **2022**, *13*, DOI 10.1038/s41467-021-27752-0.
[24] R. He, T. Kyu, *Macromolecules* **2016**, *49*, 5637–5648.
[25] G. Homann, L. Stolz, M. Winter, J. Kasnatscheew, *iScience* **2020**, *23*, 101225.
[26] L. Seidl, R. Grissa, L. Zhang, S. Trabesinger, C. Battaglia, *Adv. Mater. Interfaces* **2021**, 2100704.
[27] G. Hernández, I. L. Johansson, A. Mathew, C. Sångeland, D. Brandell, J. Mindemark, *J. Electrochem. Soc.* **2021**, *168*, 100523.
[28] N. Paranjape, P. C. Mandadapu, G. Wu, H. Lin, *Polymer* **2017**, *111*, 1–8.
[29] R. Khurana, J. L. Schaefer, L. A. Archer, G. W. Coates, *J. Am. Chem. Soc.* **2014**, *136*, 7395–7402.
[30] A. J. Butzelaar, P. Röring, M. Hoffmann, J. Atik, E. Paillard, M. Wilhelm, M. Winter, G. Brunklaus, P. Theato, *Macromolecules* **2021**, *54*, 11101–11112.
[31] A. J. Butzelaar, P. Röring, T. P. Mach, M. Hoffmann, F. Jeschull, M. Wilhelm, M. Winter, G. Brunklaus, P. Théato, *ACS Appl. Mater. Interfaces* **2021**, *13*, 39257–39270.
[32] A. J. Butzelaar, K. L. Liu, P. Röring, G. Brunklaus, M. Winter, P. Theato, *ACS Appl. Polym. Mater.* **2021**, *3*, 1573–1582.
[33] M. Bergman, A. Bergfelt, B. Sun, T. Bowden, D. Brandell, P. Johansson, *Electrochim. Acta* **2015**, *175*, 96–103.
[34] Z. Lin, X. Guo, Y. Yang, M. Tang, Q. Wei, H. Yu, *J. Energy Chem.* **2021**, *52*, 67–74.
[35] V. P. H. Huy, S. So, J. Hur, *Nanomaterials* **2021**, *11*, 614.
[36] N. Boaretto, L. Meabe, M. Martinez-Ibañez, M. Armand, H. Zhang, *J. Electrochem. Soc.* **2020**, *167*, 070524.
[37] J. Feng, L. Wang, Y. Chen, P. Wang, H. Zhang, X. He, *Nano Convergence* **2021**, *8*, 1–12.
[38] J. Serra Moreno, M. Armand, M. B. Berman, S. G. Greenbaum, B. Scrosati, S. Panero, *J. Power Sources* **2014**, *248*, 695–702.
[39] F. Croce, L. L. Persi, B. Scrosati, F. Serraino-Fiory, E. Plichta, M. A. Hendrickson, *Electrochim. Acta* **2001**, *46*, 2457–2461.
[40] F. Croce, G. B. Appetecchi, L. Persi, B. Scrosati, F. Croce, G. B. Appetecchi, L. Persi, B. Scrosati, *Natur* **1998**, *394*, 456–458.
[41] C. C. Tambelli, A. C. Bloise, A. V. Rosário, E. C. Pereira, C. J. Magon, J. P. Donoso, *Electrochim. Acta* **2002**, *47*, 1677–1682.
[42] J. L. Keddie, R. A. L. Jones, R. A. Cory, *Faraday Discuss.* **1994**, *98*, 219–230.
[43] P. Rittigstein, R. D. Priestley, L. J. Broadbelt, J. M. Torkelson, *Nat. Mater.* **2007**, *6*, 278–282.
[44] B. K. Choi, K. H. Shin, *Solid State Ionics* **1996**, *86–88*, 303–306.
[45] G. Dreezen, M. H. J. Koch, H. Reynaers, G. Groeninckx, *Polymer* **1999**, *40*, 6451–6463.
[46] D. Brandell, J. Mindemark, G. Hernández, *Polymer-Based Solid State Batteries*, Boston: De Gruyter, Berlin, **2021**.
[47] F. Jeschull, "bat2dat_v1.0.1", **2022**, DOI 10.5281/zenodo.7439377.
[48] L. Edman, A. Ferry, M. M. Doeff, *J. Mater. Res.* **2000**, *15*, 1950–1954.
[49] M. Marzantowicz, J. R. Dygas, F. Krok, A. Łasińska, Z. Florjańczyk, E. Zygadło-Monikowska, A. Affek, *Electrochim. Acta* **2005**, *50*, 3969–3977.
[50] M. Marzantowicz, J. R. Dygas, F. Krok, J. L. Nowiński, A. Tomaszewska, Z. Florjańczyk, E. Zygadło-Monikowska, *J. Power Sources* **2006**, *159*, 420–430.
[51] R. D. Shannon, *Acta Crystallogr.* **1976**, *32*, 751–767.
[52] L. Poudel, R. Podgornik, W. Y. Ching, *J. Phys. Chem. A* **2017**, *121*, 4721–4731.
[53] A. Memboeuf, K. Vékey, G. Lendvay, *Eur. J. Mass Spectrom.* **2011**, *17*, 33–46.
[54] T. K. Lee, R. Andersson, N. A. Dzulkurnain, G. Hernández, J. Mindemark, D. Brandell, *Batteries & Supercaps* **2021**, *4*, 653–662.
[55] A. D. Khudyshkina, P. A. Morozova, A. J. Butzelaar, M. Hoffmann, M. Wilhelm, P. Theato, S. S. Fedotov, F. Jeschull, *Zenodo* **2021**, DOI 10.5281/zenodo.5682615.
[56] J. Lopez, D. G. Mackanic, Y. Cui, Z. Bao, *Nat. Rev. Mater.* **2019**, *4*, 312–330.
[57] J. Mindemark, M. J. Lacey, T. Bowden, D. Brandell, *Prog. Polym. Sci.* **2018**, *81*, 114–143.
[58] A. D. Khudyshkina, U.-C. Rauska, A. J. Butzelaar, M. Hoffmann, M. Wilhelm, P. Theato, F. Jeschull, *Zenodo* **2023**, DOI 10.5281/zenodo.7418421.
[59] P. A. R. D. Jayathilaka, M. A. K. L. Dissanayake, I. Albinsson, B. E. Mellander, *Electrochim. Acta* **2002**, *47*, 3257–3268.
[60] Z. Yang, J. Fan, W. Xu, Z. Yang, J. Zeng, X. Cao, *Ind. Eng. Chem. Res.* **2022**, *61*, 4850–4859.
[61] U. Oteo, M. Martinez-Ibañez, I. Aldalur, E. Sanchez-Diez, J. Carrasco, M. Armand, H. Zhang, *ChemElectroChem* **2019**, *6*, 1019–1022.
[62] S. Suarez, S. Abbrent, S. G. Greenbaum, J. H. Shin, S. Passerini, *Solid State Ionics* **2004**, *166*, 407–415.
[63] J. H. Shin, S. S. Jeong, K. W. Kim, S. Passerini, *Solid State Ionics* **2005**, *176*, 571–577.
[64] J.-H. Shin, F. Alessandrini, S. Passerini, *J. Electrochem. Soc.* **2005**, *152*, A283.
[65] K. Karthik, R. Murugan, *Ionics* **2019**, *25*, 4703–4711.
[66] U. Oteo, M. Martinez-Ibañez, I. Aldalur, E. Sanchez-Diez, J. Carrasco, M. Armand, H. Zhang, *ChemElectroChem* **2019**, *6*, 1019–1022.
[67] M. L. Fisher, M. Colic, M. P. Rao, F. F. Lange, *J. Am. Ceram. Soc.* **2001**, *84*, 713–718.
[68] E. Quartarone, P. Mustarelli, *Chem. Soc. Rev.* **2011**, *40*, 2525.
[69] G. Homann, L. Stolz, J. Nair, I. C. Laskovic, M. Winter, J. Kasnatscheew, *Sci. Rep.* **2020**, *10*, 1–9.
[70] G. Homann, L. Stolz, K. Neuhaus, M. Winter, J. Kasnatscheew, *Adv. Funct. Mater.* **2020**, *30*, 2006289.
[71] H. Wang, D. Zhai, F. Kang, *Energy Environ. Sci.* **2020**, *13*, 4583–4608.
[72] J. Mindemark, B. Sun, E. Törmä, D. Brandell, *J. Power Sources* **2015**, *298*, 166–170.
[73] C. Sångeland, R. Younesi, J. Mindemark, D. Brandell, *Energy Storage Mater.* **2019**, *19*, 31–38.
[74] W. R. Brant, R. Mogensen, S. Colbin, D. O. Ojwang, S. Schmid, L. Häggström, T. Ericsson, A. Jaworski, A. J. Pell, R. Younesi, *Chem. Mater.* **2019**, *31*, 7203–7211.
[75] B. Sun, J. Mindemark, K. Edström, D. Brandell, *Solid State Ionics* **2013**, 2–6.
[76] F. Jeschull, *Zenodo* **2022**, DOI 10.5281/zenodo.7439377.

Manuscript received: September 15, 2023
Revised manuscript received: October 29, 2023
Accepted manuscript online: October 30, 2023
Version of record online: November 13, 2023